Original Article
Cite This: Colloid & Nanoscience Journal 1 (2023) 102-111.
CNJ.araku.ac.ir

Synthesis and characterization of NaP zeolite@Fe_3O_4 nanocomposite functionalized with 2-aminopyridine as a micro-meso structure

Zohreh Mortezaei[*1], Mojgan Zendehdel[1]

Received:2023-04-17
Revised: 2023-05-16
Accepted: 2023-05-21
DOI: **10.52547/CNJ.1.2.103**

[1]Department of Chemistry, Faculty of Science, Arak University, Arak 38456-8-8349, Iran

Abstract

Nowadays, overcome to agglomeration of nanoparticles is one of the most important problems in catalytic reaction. In this way, Fe_3O_4 nanoparticles introduced to zeolite gel as a template and magnetic nanocomposite of NaP zeolite@Fe_3O_4 with different ratio were prepared, then in the second step to prepare acid-base catalyst NaP zeolite@Fe_3O_4 functionalized with 2-aminopyridine as a basic group. Several techniques were used to evaluate the physical and chemical characterizations magnetic acid and base nanocomposites. The X-ray diffraction (XRD) confirm the presence of NaP zeolite and Fe_3O_4 in the composite. The Scanning electron microscope (SEM) graphs showed that much of Fe_3O_4 was successfully coated by the NaP zeolite layer. Also, the Vibrating sample magnetometer (VSM) results show that the magnetism of the products is stable even with introducing Fe_3O_4 to zeolite. The Transmission electron microscopy (TEM) and Burner Emmet Taller (BET) confirmed the presence of mesoporous phase in the surface of NaP zeolite@Fe_3O_4 and preparation a micro-meso structure.

Keywords: Zeolite, Magnetic nanocomposite, Aminopyridine, Mesoporous phase

1. Introduction

In the industry sector, it is important to design new and highly efficient catalysts for the synthesis of organic compounds based on the principles of green chemistry. Also, the preparation of heterogeneous catalyst which recover and reuse has been a long goal in catalyst research. Recent studies have shown that hybrid materials such as Inorganic–Inorganic or Inorganic-organic material widely used as a heterogeneous catalyst for organic reactions and antimicrobial agent [1-10].

During the recent years, increasing attention has been paid to the use of magnetic nanoparticles (MNPs) as support. One of the important magnetic materials is magnetite (Fe_3O_4) which has a spinel structure. This magnetic nanoparticle is usually promising as a catalyst for organic synthesis due to its high efficiency and easy separation from aqueous solution [7,8]. It is well known that magnetic particles which synthesized by different methods are usually agglomerated and their specific area and catalytic efficiency decreased [9,10]. An effective method to prevent the agglomeration is dispersing of particles on a stable support. The porous materials, such as zeolites can be used as a support for different materials. The zeolites are a crystalline aluminosilicate with well-defined channel and cavity, good acidity, high surface areas [11]. However, introducing of Fe_3O_4 to zeolite may be decreased the catalytic activity due to diffusion limitation of microporous, but increasing of acidity and preparation of a recoverable catalysts are more important for many organic reactions. There are many reports which shows the surface of MNPs functionalized by different materials such as organic, organometallic and acidic groups which useful for many organic reactions [12]. Although the surface of the MNPs and zeolite with free silanol groups (Si-OH) are suitable agents for functionalization [13,14] but immobilizing of amine groups to zeolite/Fe_3O_4 has not yet been reported. The goal of the present study is design and develop a new hybrid from zeolite@Fe_3O_4 that functionalize by 2-aminopyridine (NaP zeolite@Fe_3O_4/Am-Py) which can be used as a bifunction acid and base catalyst. All of samples and also the prepared nanocomposite were characterized with several analysis such as XRD, FT-IR, EDAX, SEM, TG/DT, TEM, BET and VSM.

Corresponding Authors:
zeo.sercher@yahoo.com

2. Experimental

2.1. Materials

The materials such as $FeCl_3.6H_2O$, $FeCl_2.4H_2O$, NH_3 (25%), toluene, chloroform and ethanol were purchased from Merck. Also, organic compounds included 3-chloropropyltrimethoxysilane and 2-aminopyridine purchased from Aldrich.

2.2. Synthesis of Fe_3O_4 nanoparticles

Fe_3O_4 nanoparticles were synthesized by coprecipitation of $FeCl_3.6H_2O$ (4.7 g) and $FeCl_2.4H_2O$ (1.7 g) at the molar ratio of following condition (Fe^{3+} : Fe^{2+} = 2:1), and they were dissolved in deionized water. After stirring for 30 min (80 °C), NH_3 (25%) was added to the solution under N_2 atmosphere. The Fe_3O_4 nanoparticle filtered and washed five times with deionized water and then dried under vacuum at 50 °C for 24 h [15].

2.3. Synthesis of NaP zeolite@Fe_3O_4 nanocomposites

Different amount of Fe_3O_4 (0.125, 0.250, 0.375, 0.500 g) were added to a fresh gel of zeolite with the molar composition of 320 H_2O: 16 NaOH : 1 $Al(OH)_3$: 15 SiO_2 which agitation for 5 days and stirred for 5 hours and finally placed in an autoclave at 100 ^{0}C for 24 h. After cooling the reaction mixture to room temperature, the solid product NaP zeolite@Fe_3O_4 composite filtered and washing with water until pH=9 and drying in air [15].

2.4. Synthesis of NaP zeolite@Fe_3O_4/Am-Py nanocomposites

In the first step, 1 mmol of 3-chloropropyltrimethoxysilane (3-ClPTMS) was reacted with 1.2 mmol 2-aminopyridine in 5 mL dry toluene and refluxing at 90 °C under nitrogen atmosphere for 30 h. The resulting material (PTMS-Py) was added to 0.5 g of NaP zeolite/Fe_3O_4 in 10 mL toluene (dry) and refluxing for 24 h under nitrogen atmosphere. Finally, the solid product NaP zeolite @Fe_3O_4/Am-Py was filtered, washed by chloroform, ethanol and water, respectively and dried at 100 °C for 24 h [16].

2.5. Characterization

The patterns of X-ray diffraction (XRD) were recorded by an X-Ray diffractometer (Philips 1840) with Cr-Kα radiation for analysis of pure Fe_3O_4 nanoparticles, NaP zeolite@Fe_3O_4 (1:2), NaP zeolite@Fe_3O_4/Am-Py. Fourier Transfer Infrared (FT-IR) analysis were record by a Galaxy series FT-IR 5000 spectrometer. The chemical compositions of the samples were determined by Energy-dispersive X-ray spectroscopy (EDAX) (Oxford X-max). To study the morphological of the prepared samples, the Scanning Electron Microscope (SEM) images were obtained using a Zeiss Sigma-VP FESEM instrument. The thermal analysis was performed using a Diamond Pyris TM, TG/DT 6300 from 25 to 900 °C at a heating rate of 10 °C/min under Argon flow for investigation of the theram stability ot the prepared nanocomposite. Burner Emmet Taller apparatus (SIBATA, App,1100-SA with adsorption of nitrogen at 76.34° K) was used. The VSM analysis was carried out by AGFM operation and EM900/ZISS.

3. Results and discussion

3.1. FT-IR spectra

The FT-IR spectra for pure Fe_3O_4 nanoparticles, NaP zeolite@Fe_3O_4 (1:2), NaP zeolite@Fe_3O_4/Am-Py (1:2) are shown in Fig. 1. The result show that the Fe-O stretching vibrations about 388 and 580 cm^{-1} cans be observed for Fe_3O_4 nanoparticles which hidden with the broad band related to zeolite after creating zeolite@Fe_3O_4. As can be seen from this Fig. 1, the significant change observed with introducing Fe_3O_4 nanoparticles to zeolite which the appearance of the peaks about 1007 cm^{-1} attributable to the asymmetric stretching of Al–O–Si chain and the symmetric stretching and bending frequency bands of Al–O–Si framework of zeolite (743 and 436 cm^{-1}, respectively) confirmed the present of zeolite in the NaP zeolite@Fe_3O_4/Am-Py nanocomposite [17]. Several bonds about 1439, 2958 and 3450 cm^{-1} related to C-N, C-H and N-H groups can be attributed the characteristic absorption of alkylamino pyridine [18]. The peaks at 3300-3700 and 1625 cm^{-1} related to O-H stretching and deformed vibration were observed.

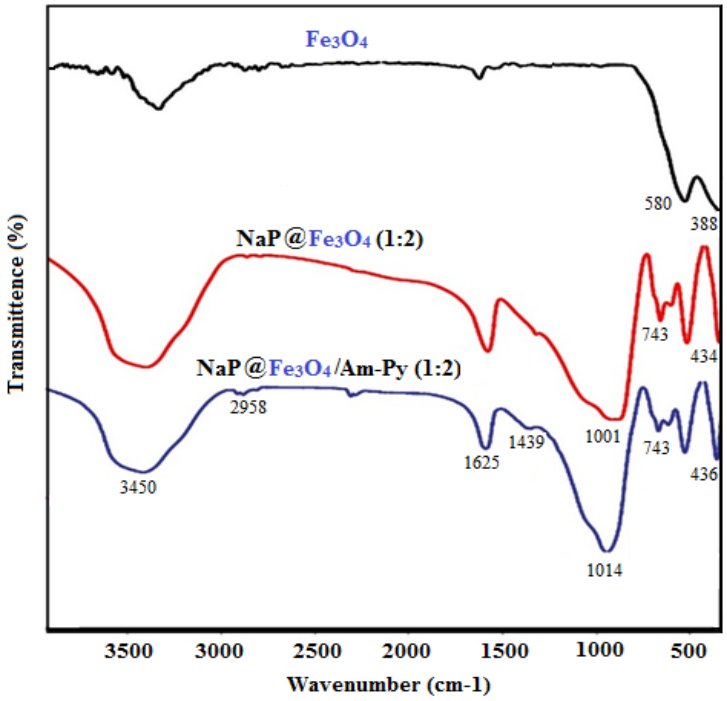

Fig. 1. The FT-IR spectra for pure Fe_3O_4, zeolite@Fe_3O_4 (1:2) and zeolite@Fe_3O_4/Am-Py (1:2).

3.2. XRD analysis

The XRD patterns of Fe_3O_4, zeolite@Fe_3O_4 and zeolite@Fe_3O_4/Am-Py were investigated (Fig. 2). We can be observed six characteristic peaks at the 2Θ values of 18.6˚, 31.6˚, 36.0˚, 44.6˚, 54.1˚, 57.3˚, which (1 1 1), (2 2 0), (3 1 1), (4 0 0), (4 2 2), (5 1 1) and (4 4 0) reflections, respectively could be attributed to it and confirm presence of cubic reverse spinel phase of Fe_3O_4 (JCPDS 653107) [19].

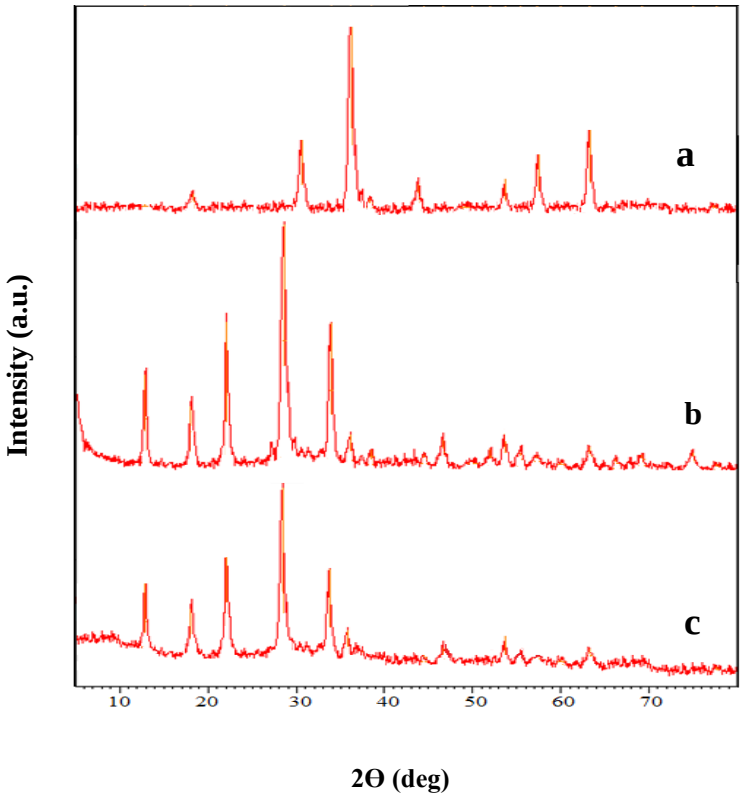

Fig. 2. The XRD patterns of Fe_3O_4 (a) zeolite@Fe_3O_4 (b) zeolite@Fe_3O_4/Am-Py (c)

After introducing different amounts of Fe_3O_4 to zeolite, all the composites show similar characteristic peaks (2θ = 12.48˚, 17.92˚, 21.79˚, 28.1˚and 33.4˚) related to the presence of NaP zeolite beside the magnetic phase (JCPDS 710962) [20] and decreasing of intensity for it suggests that some of this MNPs incorporated to the zeolite which in agreement to other reports [18,21,22].
Also, the result show that after functionalize NaP zeolite@Fe_3O_4 nanocomposite by alkylamino pyridine due to interaction of 3-ClPTMS with zeolite small amount of amorphous phase can be observed [9].
The crystallite size of these as-synthesized Fe_3O_4 in the composite with different percent was estimated from the full width at half maximum (FWHM) of strongest diffraction peak 2θ = 31.6 using the Scherrer's equation [23], $D = 0.9\lambda/(\beta \text{ Cos } 2\theta)$ where D is the crystallite size, λ is the wavelength of Cr-Kα radiation, β is FWHM, and θ is the diffraction angle of the strongest characteristic peak. The data show that the crystallite size of MNPs was increased from 13 to 40 nm when introduced to composite which may be due to agglomeration.

3.3. SEM, EDX and TEM analysis

Fig.3 show that the SEM images of the Fe_3O_4 nanoparticles and NaP zeolite@Fe_3O_4 with 1:2 ratio and NaP zeolite@Fe_3O_4/Am-Py (1:2). Therefore, in Fig. 3a the spherical structure was shown for Fe_3O_4 nanoparticles that exhibit a rough surface and average diameter of about 13 nm. After introducing magnetic nanoparticles of Fe_3O_4 into zeolite wool ball-like [24] morphology was observed for 1:2 (Fig. 3b) ratios and also spherical MNPs presence. For NaP zeolite@Fe_3O_4 (1:2) with higher percent of MNPs small agglomeration can be observed for it (Fig. 3c). The image for NaP zeolite@Fe_3O_4/Am-Py with 1:2 ratio in Fig. 3d show the morphology of NaP zeolite doesn't change but the percent of amorphous phase increased.
The chemical composition of the related compounds was considered by EDAX and elemental analysis (Tab. 1). The result for the C/N and Si/Al for all samples are very close to real ratios for materials which confirmed the present of NaP zeolite, Fe_3O_4 and alkylamino pyridine in the nanocomposite.

The size and shape of NaP zeolite@Fe_3O_4 (1:2) and NaP zeolite@Fe_3O_4/Am-Py (1:2) were observed in Fig. 4 using high resolution TEM. The images show that the quasi-spherical Fe_3O_4 with average diameter about 33 nm completely dispersed on zeolite in the 1:2 ratios without any agglomeration, but with increasing the percent of Fe_3O_4, in some parts agglomeration can be seen. Also, after functionalization of NaP zeolite@Fe_3O_4 with aminopyridine moiety, mesoporous phase was decreased which confirm the small amounts of amorphous phase which observed in XRD and decreasing of $\mathbf{S_{meso}}$ in BET [18,25].

Table 1. The elemental analysis of compounds

Sample	% C	% N	% O	% Fe	% Si	% Al	C/N	Si/Al
Fe_3O_4	-	-	48.53	51.47	-	-	-	-
NaP zeolite@Fe_3O_4 (1:2)	-	-	45.89	14.23	22.68	11.45	-	1.98
NaP zeolite@Fe_3O_4/Am-Py (1:2)	10.21	4.28	55.42	6.39	17.02	6.68	2.38	2.55

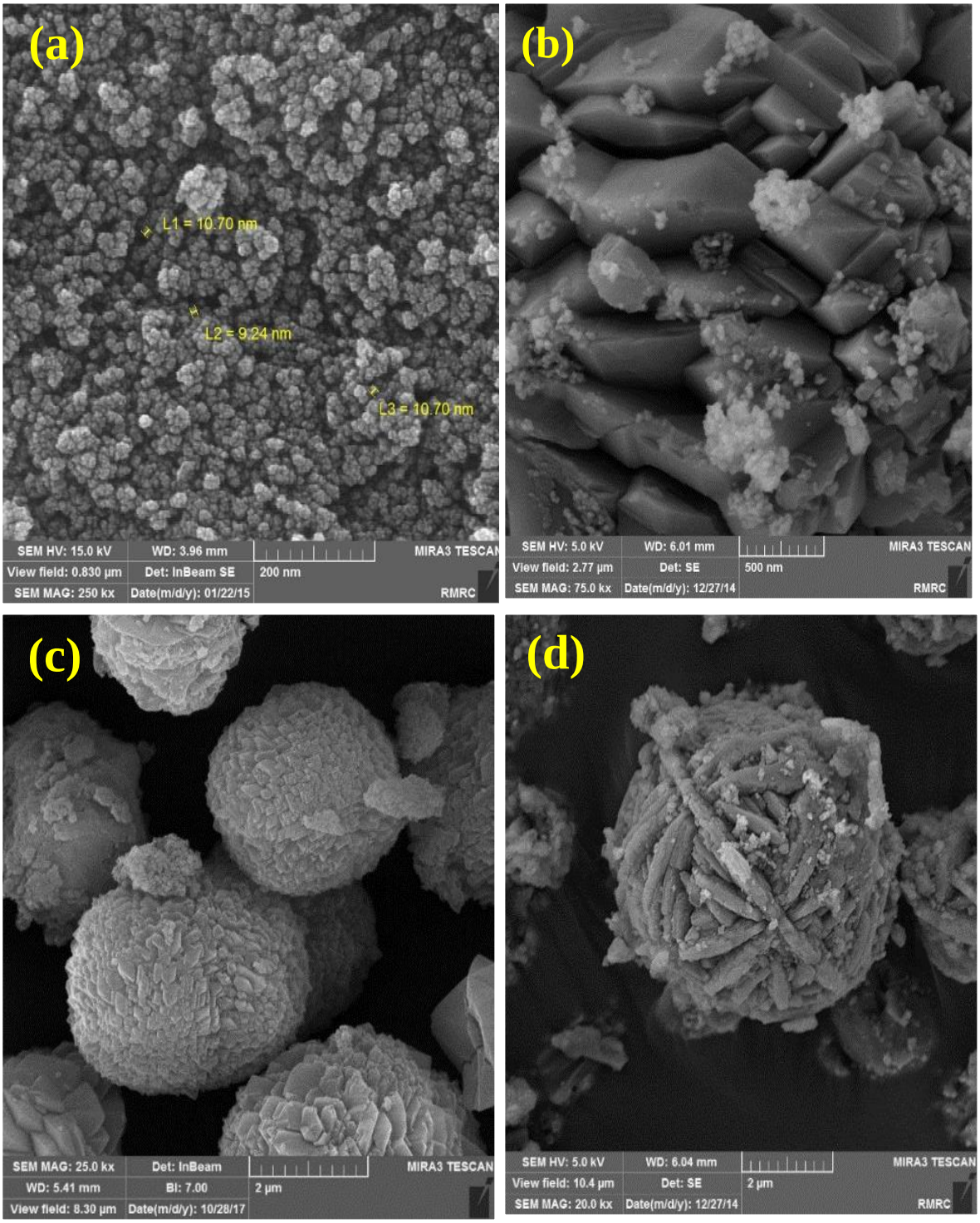

Fig. 3. The SEM images of the Fe_3O_4 (a) nanoparticles and NaP zeolite@Fe_3O_4 with 1:2 ratio before(b) and after functionalize with amine (c,d)

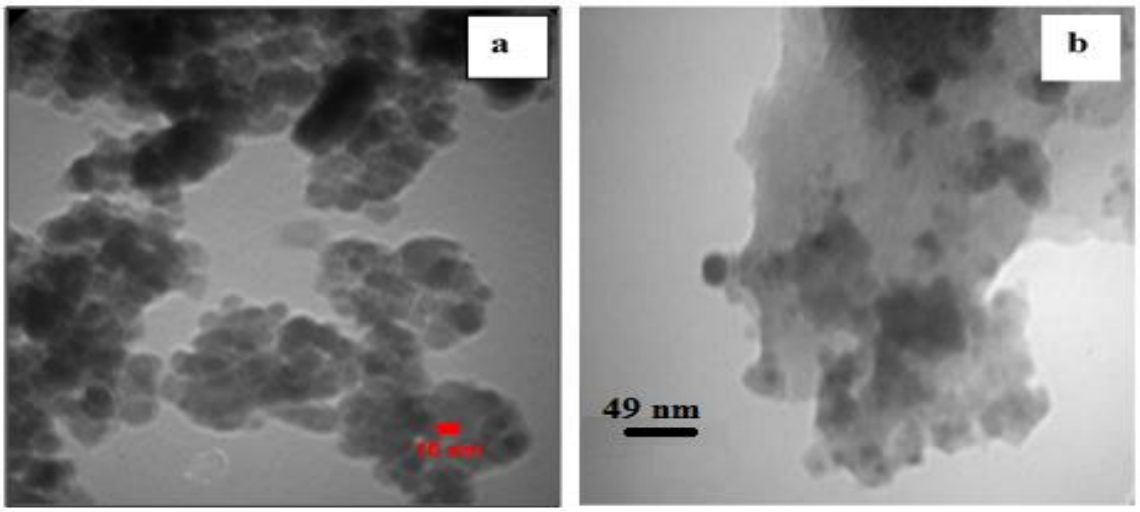

Fig. 4. The TEM images of the NaP zeolite@Fe_3O_4 (1:2) before(a) and after functionalize with amine (b)

3.4. BET analysis

Fig. 5 shows the Nitrogen adsorption/desorption isotherm and the pore size distribution of NaP zeolite@Fe_3O_4 with 1:2 percent before (a) and after functionalize with amine (b). A sudden increasing in the N_2 isotherm at the low-pressure region about P/P0 < 0.1 confirmed the existence of micropores phase [26]. Also, presence of hysteresis loop at pressure P/P0 of 0.5-1, that is the type-IV isotherm, indicate the mesoporous phase [27]. The result show that after functionalize NaP zeolite@Fe_3O_4 with amine (Fig. 5b) the micro phase decreasing and also a rapid increasing at high-pressure region about P/P0＞0.9, suggested the existence of macropores phase [28]. The remarkable decrease in the pore volume and pore area of NaP zeolite@Fe_3O_4 after functionalize by alkylamino pyridine can be attributed to the introducing of amine into the nanocomposite.

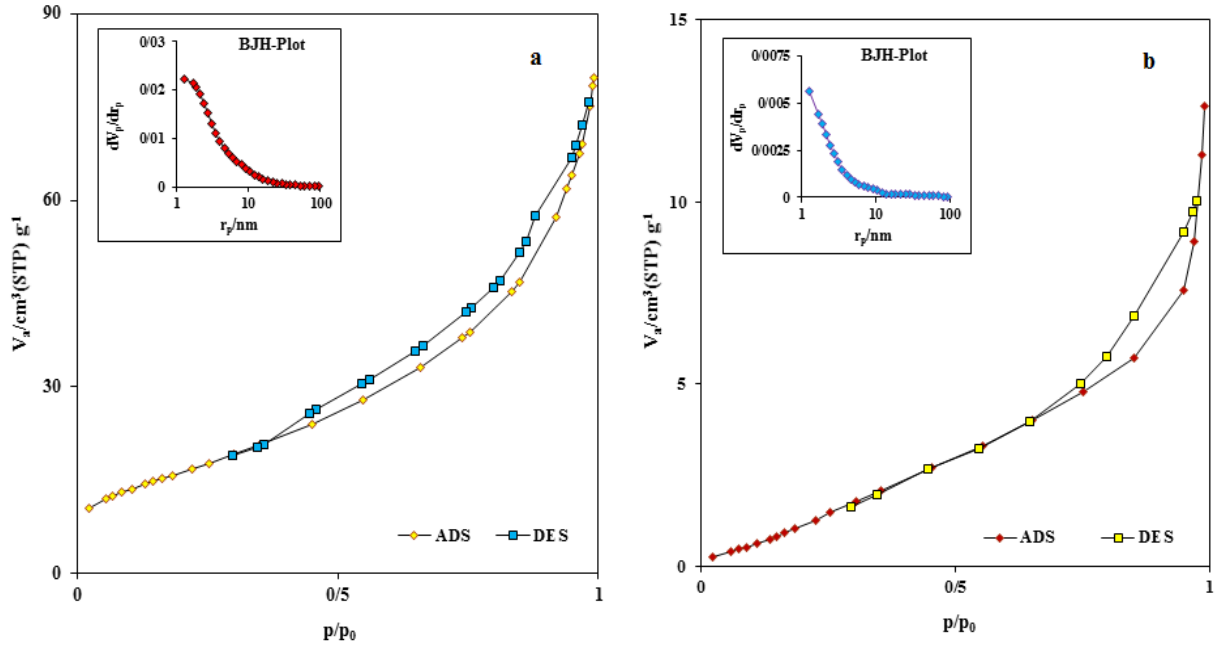

Fig. 5. Nitrogen adsorption/desorption isotherms and BJH Plot of NaP zeolite@Fe_3O_4 (1:2) (a) and NaP zeolite@Fe_3O_4/Am-py (1:2) (b)

Also, the result in Tab. 2 were calculated using BET, BJH, and t-Plot methods show that the surface area for NaP zeolite (45 m^2/g) increased after introducing Fe_3O_4 in the framework due to increasing mesophase which these results may be confirmed the present of hierarchical structure for zeolite. The pore size distribution result in Fig. 5 (a, b) for all cases show two ranges of particle size 1-8 nm corresponding to mesoporous materials and greater than 8 nm related to microporous phase the confirmed this conclusion [9,29].

Table 2. The BET data of samples

Sample	S_{BET} (m^2/g)	S_{micro} (m^2/g)	S_{meso} (m^2/g)	V_t (cm^3/g)	V_{micro} (cm^3/g)	V_{meso} (cm^3/g)
NaP zeolite@Fe_3O_4 (1:2)	129.15	60.31	68.84	0.28	0.09	0.14
NaP zeolite@Fe_3O_4 /Am-Py (1:2)	48.57	18.89	29.68	0.09	0.04	0.03

[a] Calculated by the BET method.
[b] Calculated by the t-plot method.
[c] Obtained at a relative pressure of 0.99.
[d] Calculated by the BJH method

3.5. Thermal Analysis

The TGA-DTG curves of the NaP zeolite@Fe_3O_4 and NaP zeolite@Fe_3O_4/Am-Py (1:2) samples before and after functionalize with amine were investigated. The TGA curves which can be divided into three steps. For NaP zeolite@Fe_3O_4, the first weight loss (11.9%) in 25-200 ^{0}C is attributed to the removal of physiosorbed and chemisorbed water. The second step, weight loss (4.7%) in 200-580 ^{0}C attributed to NaP zeolite phase transfer [30]. The third step, weight loss (1.4%) in 580-900 $^\circ$C, accompanied with endothermic peaks in DTG can be corresponded to the dehydration of the hydroxyl groups inside the micro and meso phases [31] and also changing in the structure of Fe_3O_4 present in this region [32]. In the case of NaP zeolite@Fe_3O_4/Am-Py the percent of weight loss in the second steps increased about 3.7% due to thermal decomposition of the organic agent and also in the DTA curves two peaks endothermic can be seen which, the first peak about 200-300 ^{0}C confirmed the presence of alkylamino pyridine in the structure [33]. The last steps might be related to some transformations of phase of Gismondine-like structures and Fe_3O_4, respectively [18,34,35].

3.6. VSM analysis

The magnetic properties of Fe_3O_4 nanoparticles, NaP zeolite@Fe_3O_4, and NaP zeolite@Fe_3O_4/Am-Py nanocomposites were investigated using a vibrating sample magnetometer (VSM) from -10000 to +10000 Oe (Fig. 6). The results show that the saturation magnetizations of the Fe_3O_4 MNPs is about 13.06 % of the Fe_3O_4 bulk materials value (Tab. 3). When MNPs introduced to NaP zeolite with different ratio and also after functionalize amine decreased. These results may be due to i) increasing size of MNps after introduce to zeolite ii) high interaction between Fe_3O_4 nanoparticles and zeolite iii) and covering of nanoparticles by zeolite and alkylamino pyridine [36,37]. Also, the shape of slope the magnetic hysteresis loops confirmed that all materials exhibit very low remanence (Mr) at ambient temperature and indicating superparamagnetic behavior for all samples [30].

Table 3. The magnetic properties of Fe_3O_4, NaP zeolite@Fe_3O_4, and NaP zeolite@Fe_3O_4/Am-Py samples

Sample	Ms (emu/g)	Hc (Oe)
Fe_3O_4	60.00	0
NaP zeolite@Fe_3O_4 (1:2)	7.84	0
NaP zeolite@Fe_3O_4/Am-Py (1:2)	5.62	0

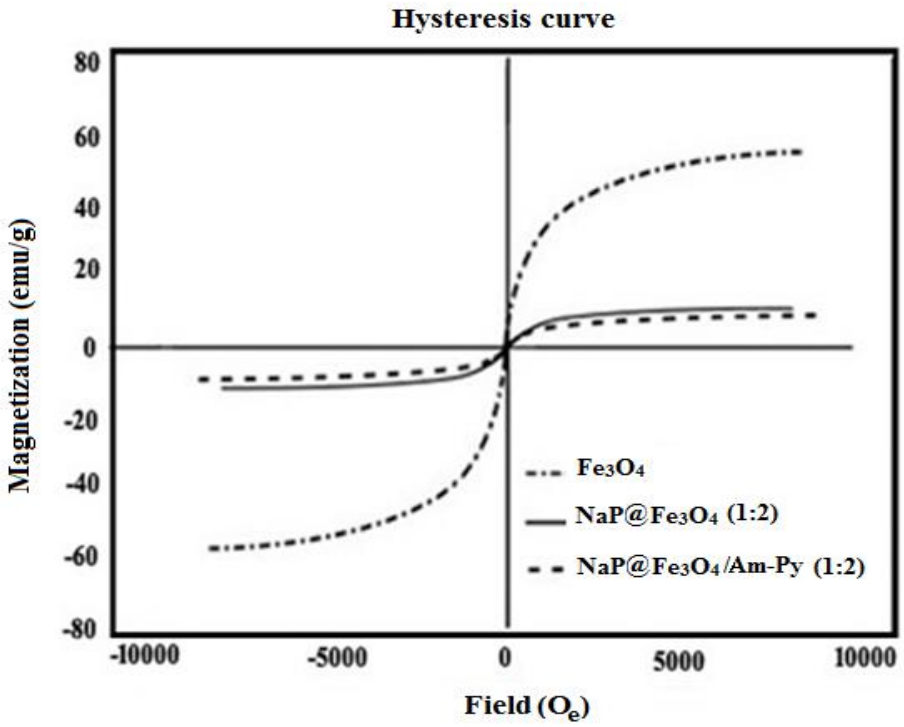

Fig. 6. Magnetic hysteresis curves of Fe_3O_4, NaP zeolite@Fe_3O_4 and NaP zeolite@Fe_3O_4/Am-Py.

4. Conclusion

The Fe_3O_4 magnetic nanoparticles, with uniformly distributed 13 nm size were synthesized. These nanoparticles with different ratios introduced to gel of zeolite and under hydrothermal condition. Then a micro-meso structure of zeolite was prepared and the NaP zeolite@Fe_3O_4 nanostructure functionalized with 2-aminopyridine as a basic organic moiety. The structure of hybrid nanostructure was confirmed by FT-IR, XRD, BET, VSM, TGA, SEM and TEM techniques. The SEM graphs showed that much of Fe_3O_4 was successfully coated by the NaP zeolite layer. Also, the results show that the magnetism of the products is stable with added zeolite. These particles show perfectly uniform sphere, and the aggregation of the nanoparticles can be discerned clearly.

Conflicts of Interest

The author declares no conflict of interest.

Acknowledgment

Thanks to the Research Council of Arak University and Center of Excellence in the Chemistry Department of Arak University for supporting of this work.

Author information

*Corresponding Author: Zohreh Mortezaei
E-mail address: zeo.sercher@yahoo.com

ORCID
Mojgan Zendehdel: 0000-0002-1364-5660

References

[1] M. Ghanbari, M. Salavati-Niasari, $T_{l4}CdI_6$ Nanostructures: Facile Sonochemical synthesis and photocatalytic activity for removal of organic dyes, Inorg. Chem. 57(18) (2018) 11443–11455. https://doi.org/10.1021/acs.inorgchem.8b01293.

[2] J. Ma, B. Zhou, F. Chen, K. Pan, How marine diatoms cope with metal challenge: Insights from the morphotype-dependent metal tolerance in Phaeodactylum tricornutum, Ecotoxicol. Environ. Saf. 208 (2021) 111715. https://doi.org/10.1016/j.ecoenv.2020.111715.
[3] M. Karami, M. Ghanbari, H. A. Alshamsi, S. Rashkic, M. Salavati-Niasari, Facile fabrication of Tl_4HgI_6 nanostructures as novel antibacterial and antibiofilm agents and photocatalysts in the degradation of organic pollutants, Inorg. Chem. Front. 8 (2021) 2442-2460. https://doi.org/10.1039/D1QI00155H.
[4] M. Hosseini, M. Amiri, M. Ghanbari, M. A. Mahdi, W. K. Abdulsahib, M. Salavati-Niasari, Drug delivery based on chitosan, β-cyclodextrin and sodium carboxymethyl cellulose as well as nanocarriers for advanced leukemia treatment, Biomed. Pharmacother. 153 (2022) 113369. https://doi.org/10.1016/j.biopha.2022.113369.
[5] M. Karami, M. Ghanbari, O. Amiri, M. Salavati-Niasari, Enhanced antibacterial activity and photocatalytic degradation of organic dyes under visible light using cesium lead iodide perovskite nanostructures prepared by hydrothermal method, Sep. Purif. Technol. 253 (2020) 117526. https://doi.org/10.1016/j.seppur.2020.117526
[6] A. Panahi, M. Ghanbari, E. A. Dawi, R. Monsef, R. R. Abass, A. M. Aljeboree, M. Salavati-Niasari, Simple sonochemical synthesis, characterization of $TmVO_4$ nanostructure in the presence of Schiff-base ligands and investigation of its potential in the removal of toxic dyes, Ultrason. Sonochem. 95 (2023) 106362. https://doi.org/10.1016/j.ultsonch.2023.106362.
[7] Y. Chen, J. Sun, Y. Zhang, Sh. Zheng, B. Wang, Z. Chen, Y. Xue, M. Chen, M. Abbas, J. Chen, $CoFe_2O_4$ nanoarray catalysts for Fischer-Tropsch synthesis, J. Fuel. Chem. Technol. 45 (2017) 1082-1087. https://doi.org/10.1016/S1872-5813(17)30050-6.
[8] Y. Wei, B. Han, X. Hu, Y. Lin, X. Wang, X. Deng, Synthesis of Fe_3O_4 nanoparticles and their magnetic properties, Procedia Eng. 27 (2012) 632-637. https://doi.org/10.1016/j.proeng.2011.12.498.
[9] Y. Du, W. Ma, P. Liu, B. Zou, J. Ma, Magnetic $CoFe_2O_4$ nanoparticles supported on titanate nanotubes ($CoFe_2O_4$/TNTs) as a novel heterogeneous catalyst for peroxy mono sulfate activation and degradation of organic pollutants, J. Hazard. Mater. 308 (2016) 58–66. https://doi.org/10.1016/j.jhazmat.2016.01.035.
[10] Y. Wang, H. Zhao, M. Li, J. Fan, G. Zhao, Magnetic ordered mesoporous copper ferrite as a heterogeneous Fenton catalyst for the degradation of imidacloprid, Appl. Catal. B: Environ. 147 (2014) 534–545. https://doi.org/10.1016/j.apcatb.2013.09.017.
[11] M. Zendehdel, A. Mobinikhaledi, Z. Mortezaei, Host (nano cage of zeolite Y)/guest transition metal complexes of N, N-bis (salicylidene)4,5-dimethyl-1,2-phenylenediamine: Synthesis, characterization, catalytic activity for oxidation of phenol and kinetic study, J. Iran. Chem. Soc. 12 (2015) 283-292. https://doi.org/10.1007/s13738-014-0483-x.
[12] C. S. Gill, B. A. Price, C. W. Jones, Sulfonic acid-functionalized silica-coated magnetic nanoparticle catalysts, J. Catal. 251 (2007) 145–152. https://doi.org/10.1016/j.jcat.2007.07.007.
[13] C. M. Crudden, M. Sateesh, R. Lewis, Mercaptopropyl-modified mesoporous silica: a remarkable support for the preparation of a reusable, heterogeneous palladium catalyst for coupling reactions, J. Am. Chem. Soc. 127 (2005) 10045-10050. https://doi.org/10.1021/ja0430954.
[14] X. S. Zhao, G.Q. Lu, A.K. Whittaker, G.J. Millar, H.Y. Zhu, Comprehensive study of surface chemistry of MCM-41 using 29Si CP/MAS NMR, FTIR, Pyridine-TPD, and TGA, J. Phys. Chem. B. 101 (1997) 6525-6531. https://doi.org/10.1021/jp971366.
[15] M. Zendehdel, M. Ramezani, B. Shoshtari-Yeganeh, G. Cruciani, A. Salmani, Simultaneous removal of Pb (II), Cd (II) and bacteria from aqueous solution using amino functionalized Fe_3O_4/NaP zeolite nanocomposite, Environ. Technol. 40 (2018) 1-50. https://doi.org /10.1080/09593330.2018.1485750.
[16] M. Esmaeilpour, J. Javidi, F. Nowroozi Dodeji, M. Mokhtari Abarghoui, Facile synthesis of 1- and 5-substituted 1H-tetrazoles catalyzed by recyclable ligand complex of copper (II) supported on superparamagnetic Fe_3O_4@SiO_2 nanoparticles, J. Mol. Catal. A: Chem. 393 (2014) 18-29. https://doi.org/10.1016/j.molcata.2014.06.001.
[17] D. Chandra, T. Yokoi, T. Tatsumi, A. Bhaumik, Highly Luminescent organic-inorganic hybrid mesoporous silicas containing tunable chemosensor inside the pore wall, Chem. Mater. 19 (2007) 5347–5354. https://doi.org/10.1021/cm701918t.
[18] Z. Mortezaei, M. Zendehdel, M. A. Bodaghifard, Cu complex grafted on the porous materials: synthesis, characterization and comparison of their antibacterial activity with nano‑Cu/NaY zeolite, J. Iran. Chem. Society. 17 (2020) 283–295. https://doi.org/10.1007/s13738-019-01769-1.
[19] J. K. Rajput, G. Kaur, Synthesis and applications of $CoFe_2O_4$ nanoparticles for multicomponent reactions, Catal. Sci. Technol. 4 (2014) 142–151. https://doi.org/10.1039/C3CY00594A.
[20] S. Hansen, U. Hakansson, L. Faelth, Structure of synthetic zeolite Na-P2, Section C: Crystal Structure Communications. 46 (1990) 1361-1362. https://doi.org/10.1107/S010827018901262X.

[21] A.H. Alwash, A.Z. Abdullah, N. Ismail, Zeolite Y encapsulated with Fe-TiO_2 for ultrasound-assisted degradation of amaranth dye in water, J. Hazard. Mater. 233-234 (2012) 184-193. https://doi.org/10.1016/j.jhazmat.2012.07.021.
[22] K. Na, M. Choi, R. Ryoo, Recent advances in the synthesis of hierarchically nanoporous zeolites, Micropor. Mesopor. Mat. 166 (2013) 3–19. https://doi.org/10.1016/j.micromeso.2012.03.054.
[23] Y. Orooji, M. Ghanbari, O. Amiri, M. Salavati-Niasari, Facile fabrication of silver iodide/graphitic carbon nitride nanocomposites by notable photo-catalytic performance through sunlight and antimicrobial activity, J. hazard. Mat. 389 (2020) 122079. https://doi.org/10.1016/j.jhazmat.2020.122079.
[24] Z. Huo, X. Xu, Z. Lü, J. Song, M. He, Z. Li, Q. Wang, L. Yan, Synthesis of zeolite NaP with controllable morphologies, Micropor. Mesopor. Mat. 158 (2012) 137-140. https://doi.org/10.1016/j.micromeso.2012.03.026.
[25] J.L. Cao, X. Wu. Liu, R. Fu, Z.Y. Tan, Magnetic P zeolites: Synthesis, characterization and the behavior in potassium extraction from seawater, Sep. Purif. Technol. 63 (2008) 92–100. https://doi.org/10.1016/j.seppur.2008.04.015.
[26] J. Hou, K. Jiang, R. Wei, M. Tahir, X. G. Wu, M. Shen, X. Z. Wang, C.B. Cao, Popcorn-derived porous carbon flakes with an ultrahigh specific surface area for superior performance supercapacitors, J. ACS. Appl. Mater. Interfaces. 9 (2017) 30626-30634. https://doi.org/10.1021/acsami.7b07746.
[27] M. Fu, W. Chen, J. Ding, X. Zhu, Q. Liu, Biomass waste derived multi-hierarchical porous carbon combined with $CoFe_2O_4$ as advanced electrode materials for super capacitors J. Alloys Compd. 12(2018)244. https://doi.org/10.1016/j.jallcom.
[28] Q. Wang, Q. Cao, X.Y. Wang, B. Jing, H. Kuang, L. Zhou, A high-capacity carbon prepared from renewable chicken feather biopolymer for supercapacitors, J. Power Sources. 225 (2013) 101-107. https://doi.org/10.1016/j.jpowsour.2012.10.022.
[29] O. Mazaheri, R. J. Kalbasi, Preparation and characterization of Ni/mZSM-5 zeolite with a hierarchical pore structure by using KIT-6 as silica template: an efficient bi-functional catalyst for the reduction of nitro aromatic compounds, RSC. Adv. 5 (2015) 34398. https://doi.org/10.1039/C5RA02349A.
[30] X. Zhang, H. Niu, Y. Pan, Y. Shi, Y. Cai, Modifying the surface of Fe_3O_4/SiO_2 magnetic nanoparticles with C_{18}/NH_2 mixed group to get an efficient sorbent for anionic organic pollutants, J. Colloid. Interf. Sci. 362 (2011) 107–112. https://doi.org/10.1016/j.jcis.2011.06.032.
[31] F. Zamani, M. Zendehdel, A. Mobinikhaledi, M. Azarkish, Complexes of N, N-bis (salicylidene) 4,5-dimethyl-1,2-phenylenediamine immobilized on porous nanomaterials: Synthesis, characterization and study of their antimicrobial activity, Micropor. Mesopor. Mat. 212 (2015) 18-27. https://doi.org/10.1016/j.micromeso.2015.02.052.
[32] S. Nigam, K.C. Barick, D. Bahadur, Development of citrate-stabilized Fe_3O_4 nanoparticles: Conjugation and release of doxorubicin for the rapeutic applications, J. Magn. Magn. 323 (2011) 237-243. https://doi.org/10.1016/j.jmmm.2010.09.009.
[33] H. Zhang, Y. F. Fan, Y.H. Huan, M.B. Yue, Dry-gel synthesis of shaped transition-metal-doped M-MFI (M = Ti, Fe, Cr, Ni) zeolites by using metal-occluded zeolite seed sol as a directing agent, Micropor. Mesopor. Mat. 231 (2016) 178-185. https://doi.org/10.1016/j.micromeso.2016.06.001.
[34] A. Salabat, F. Mirhoseini, Ramin Valirasti, Engineering poly(methyl methacrylate)/Fe_2O_3 hollow nanospheres composite prepared in microemulsion system as a recyclable adsorbent for removal of benzothiophene, Ind. Eng. Chem. Res. 58 (2019) 17850-17858. https://doi.org/10.1021/acs.iecr.9b04322.
[35] Y. Yang, Y. Zhang, S. Hao, Q. Kan, Tethering of Cu(II), Co(II) and Fe(III) tetrahydro-salen and salen complexes onto amino-functionalized SBA-15: Effects of salen ligand hydrogenation on catalytic performances for aerobic epoxidation of styrene, Chem. Eng. J. 171 (2011) 1356-1366.
https://doi.org/10.1016/j.cej.2011.05.047.
[36] R. Ianoşn, M. Bosca, R. Lazău, Fine tuning of $CoFe_2O_4$ properties preparedbysolution combustion synthesis, Ceram. Int. l40 (2014) 10223–10229. https://doi.org/10.1016/j.ceramint.2014.02.110.
[37] B. J. Rani, M. Ravina, B. Saravanakumar, G. Ravi, V. Ganesh, S. Ravichandran, R. Yuvakkumar, Ferrimagnetism in cobalt ferrite ($CoFe_2O_4$) nanoparticles, Nano-Struct. Nano-Objects. 14 (2018) 84–91.
https://doi.org/10.1016/j.nanoso.2018.01.012.